CHALMERS
UNIVERSITY OF TECHNOLOGY

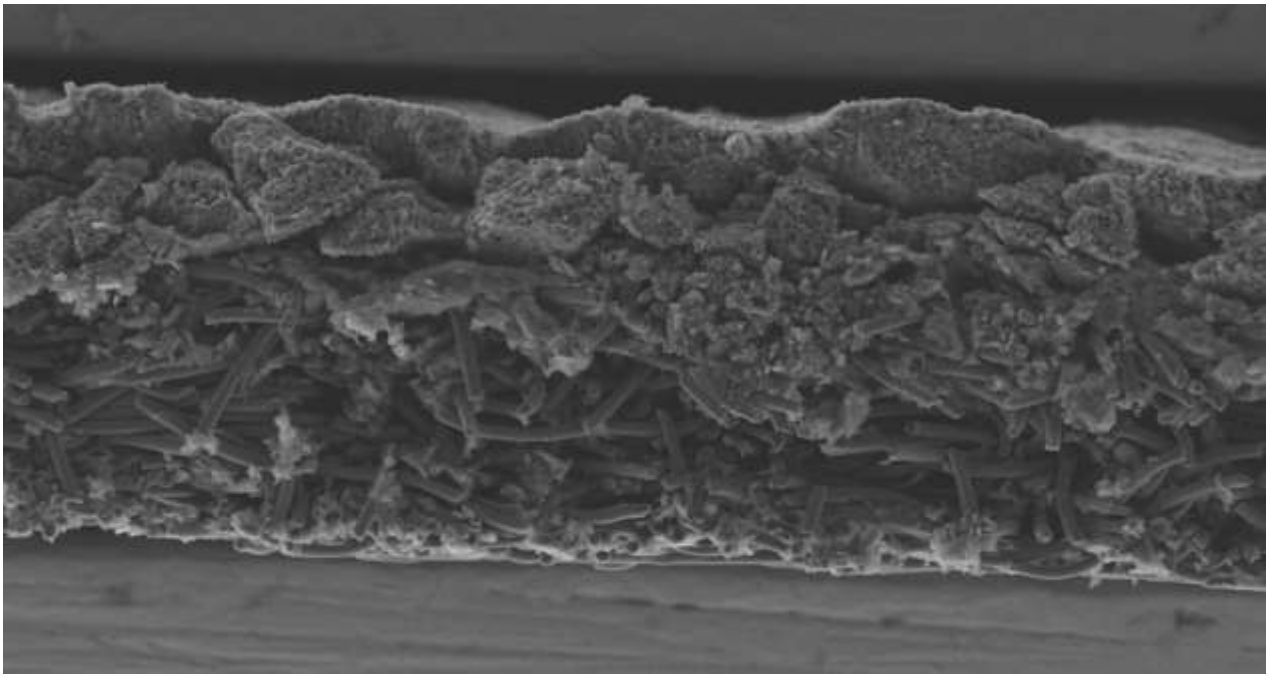

Investigating drying conditions of screen-printed platinum-free fuel cell cathode layers

Master's thesis in Materials Chemistry

Maria Rundberg

DEPARTMENT OF CHEMISTRY AND CHEMICAL ENGINEERING

CHALMERS UNIVERSITY OF TECHNOLOGY

Gothenburg, Sweden 2021
www.chalmers.se

Investigating drying conditions of screen-printed platinum-free fuel cell cathode layers

MARIA RUNDBERG

Diploma work in the Master Program Materials Chemistry

Department of Chemistry and Chemical Engineering

Chalmers University of Technology

SE-41296 Gothenburg

Tel. +46 31 772 1000

Performed at: Celcibus AB, Gruvgatan 35B, 421 30 Västra Frölunda

Supervisors: Anders Palmqvist, Chalmers University of Technology, Lisa Palmqvist and Walter Rosas Arbelaez, Celcibus AB

Examiner: Martin Andersson, Professor in Applied Chemistry, Department of Chemistry and Chemical Engineering, Chalmers University of Technology

Cover image: Scanning electron microscope image of the cathode layer after being exposed to a saturated ethanol environment followed by a slow drying in air.

Abstract

Renewable energy sources are becoming more significant in a society where sustainable development is becoming more crucial. Efficient ways to store and convert energy are therefore essential for the success implementation of the new sources. One part of the puzzle is hydrogen fuel cell technology. A challenge, however, is to develop a hydrogen fuel cell that is both cost-effective and high performing. The anode and cathode of the fuel cell are separated by a membrane, and together they are the heart of the fuel cell. The cathode side has been the focus of this study, specifically how to create a suitable coating with as minimal resistance as feasible. There are various alternative deposition procedures that may be employed; however, screen printing was used in this dissertation. The aim of this thesis is to investigating drying conditions of screen-printed platinum-free fuel cell cathode layers and minimize the ohmic resistance caused by the defects in the deposited layer. In addition, a valid resistance measurement strategy needs to be implemented and integrated during the characterization step without negatively affecting the eventual use of the membrane in fuel cell testing. The work process was divided into broad testing, reproducibility, and characterization. The samples were analyzed by microscopy techniques, profilometry and resistance measurements.

From the broad testing experiments, it could be concluded that the drying environment and time had an influence on the formation of cracks in the plane. The best possible settings found in this study were 24 hours in ethanol followed by 24 hours in slow drying air. In addition, a decreased in-plane electrical resistance could be obtained by increasing the thickness of the deposition layer. The reproducibility experiments concluded the properties of the ink also had a significant impact on resistance. Higher mass-% of dry matter resulted in increased viscosity, which aided the screen-printing process by enabling more ink to remain on the sample, resulting in a thicker deposit layer and fewer fractures. In the characterization and fuel cell experiments, tests were performed to evaluate the substrate selection closer. In general, all samples dried in air performed slightly better compared to the ones dried in a saturated environment. Possible explanations for achieving these results can be the structure of the substrate. Printing on a porous material, a portion of the ink may penetrate the substrate rather than staying on the surface as a coating. In these circumstances, the drying process benefits from a faster drying period to reduce the loss of active catalyst. Another possibility is to use a microporous sublayer as a membrane to prevent ink from entering the substrate. The third substrate evaluated, Nafion membrane, proved to be extremely fragile. Fuel cell experiments suggest that Nafion dried in air performs better, but since several samples collapsed, a controlled drying technique would be preferable. Future prospects include further optimizing the correct ink in relation to the right environment and substrate choice, increase the knowledge about Nafion membrane and how to increase the adhesion strength and investigate how the mesh marks impact the substrates.

Keywords: Platinum-free fuel cell, screen printing, cathode layers, drying environment, resistance measurements

Acknowledgements

First and foremost, I would like to thank my supervisor Anders Palmqvist for the opportunity to execute my master's thesis at the company, and for the opportunity to learn about this fascinating topic and to gain insight into the production process of Celcibus AB. I would also like to thank all the employees at Celcibus for your contributions to this diploma work and for the warm welcome.

The greatest of thanks to my supervisor in the laboratory Walter Rosas Arbelaez, for all your encouragement and support during the whole project. Thank you for always taking your time to discuss any question, the help I have received from you have been invaluable. I would also like to thank Mats Hulander, Jakob Karlsson and Viktor Eriksson at Applied Chemistry for their help and sharing of knowledge within analysing samples.

A special thank you to Lisa Palmqvist, co-founder of Celcibus AB, for the guidance and expertise that you supported with throughout the project.

A huge thank you Martin Andersson, my examiner at Chalmers University of Technology, for all the inputs, helping me pursue the project.

Finally, my sincerest thank you to my family for their constant love and support throughout my years at Chalmers University of Technology.

List of abbreviations

PG	1,2-Propandiol
CL	Catalyst Layer
GDL	Gas Diffusion Layer
MPL	Microporous Layer
PEMFC	Proton Exchange Membrane Fuel Cell

List of Figures

List of Tables

Table of content

1. Introduction

Over the previous century, the Earth's population has increased at an alarming rate, from 1.8 billion to 7.7 billion, and will most likely continue to do so throughout the twenty-first century. What is important is not the quantity itself, but the overall strain on ecosystems and natural resources [1]. Sustainability can be described as the ability "to meet present needs without compromising the ability of future generations to meet their needs" [2]. One key component in achieving this mission is to develop sustainable concepts for energy supply, storage, and conversion. Hydrogen fuel cell technology is one part of the puzzle [3]. Hydrogen can be used to store, transport, and provide energy. It is very flexible since hydrogen can be produced from all types of energy sources. Fuel cells, fuelled with hydrogen, can replace combustion engines in vehicles and when using renewable sources for the hydrogen production a zero-emission solution is obtained. Hydrogen fuel cells can also be used to provide energy to households and industrial applications.

The ability to start up fast at low temperatures is one of reasons for why PEM fuel cells are favourable. As a result, PEMFCs have gained a lot of interest from the automobile industry. To achieve hydrogen vehicle democratization, fuel cells need to become more economically desirable and simultaneously deliver a high performance [4].
Together with the two catalyst layers, the polymer membrane is the heart piece of the fuel cell. The membrane is located between the anode and cathode and plays a key role in blocking fuels, promoting proton transport, and providing necessary mechanical support for the catalytic layers. One essential step of improving the fuel cell performance is reducing the membrane ohmic resistance.

The structural features of the membrane, as well as the deposition process and drying environment, are all parameters that influence the deposition layer and the performance of the membrane in the fuel cell. Toured et al. discusses how the deposition layer thickness and mass influences the ohmic resistance [5]. Meyer et al. provide similar results and emphasize the need of establishing a homogenous layer with appropriate distribution, as well as how the number and size of fractures may affect the cell's quality [6].

1.1 Aim

The aim of this master thesis is to optimize the manufacturing process of the cathode layer on the membrane and minimize the ohmic resistance caused by the defects in the deposited layer so that the fuel cell performance can be improved. In addition, as part of the thesis, a valid resistance measurement strategy needs to be implemented and integrated during the characterization step without negatively affecting the eventual use of the membrane in fuel cell testing.

1.2 Limitations

As a consequence of time constrains, the project will be limited to focus on optimizing the preparation of the ink, the printing method, choice of substrate, drying time and the sample environment. This study will not concentrate on the synthesis of the catalyst material used in the fuel cell. Also, the fuel cell testing will be a part of the characterization process but in the scope of this thesis the fuel cell performance will not be thoroughly evaluated or optimized. The testing will follow an already established protocol.

1.3 Specification of issue under investigation

The questions to be answered in the project are:

- How to create a good sample environment to minimize the defects in the deposition layer, so the fuel cell performance can be improved?
- The correlation between the sample environment and the drying time?
- How to implement a resistance measurement strategy on samples without damaging the surface?
- Which characteristics of the ink are important in making a good printing layer?
- How does the choice of substrate influence the resistance in the cathode layer?

2. Background

2.1 Proton Exchange Membrane Fuel Cell

Fuel cells are devices that transform the chemical energy housed in a fuel directly into electricity. Apart from electricity, biproducts as water and heat are produced. The essential elements in a fuel cell are the electrodes (anode and cathode) and the electrolyte [7]. The most widely used type of fuel cell is the proton exchange membrane fuel cell (PEMFC), which is pertinent to this thesis. In PEMFC a water-based acidic polymer membrane serves as the electrolyte in the cell. The membrane separates the anode and cathode and only allows protons to pass through to the cathode side. On the anode side a catalyst divides the hydrogen molecules into protons and electrons. The electrons cannot pass the electrically non-conducting membrane and are instead led through an external circuit, where they power an electric load, and further to the cathode. At the cathode side the electrons and protons are combined with the oxygen from the air and generate water [3].

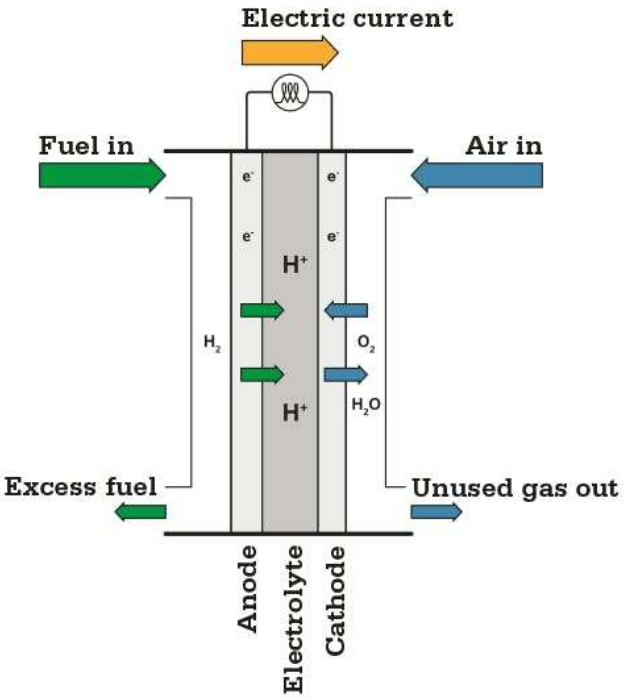

Figure 1: Components and working principle for a hydrogen fueled PEMFC [8]

The chemical reaction for a hydrogen fueled PEMFC can be written as equation 1. Equation 1 is the sum of the anode reaction (equation 2) and the cathode reaction (equation 3).

$$2H_2 + O_2 \xrightarrow{catalyst} 2H_2O \quad (1)$$

$$2H_2 \rightarrow 4H^+ + 4e^- \quad (2)$$

$$O_2 + 4H^+ + 4e^- \rightarrow 2H_2O \quad (3)$$

2.1.1 Membrane electrode assemblies (MEA)

One key component in a PEMFC is the membrane electrode assembly (MEA) consisting of the electrolyte membrane in the centre sandwiched between the two catalyst layers (CL) with gas diffusion layers (GDL) [6, 9]. The main function of the MEA is to prevent the flow of electrons and promote the flow of protons between the anode and cathode. In practice, this is accomplished by isolating the cathodic reaction from the anodic reaction using the membrane and force the electrons to go through an external circuit [10]. Several research groups have been optimizing the properties of each component in MEA in order to increase the fuel cell performance. One specific question under investigation is the structure of the GDL and how parameters as geometry and porosity will impact the optimization of gas, water, and electron transport. Another area of emphasis is the MEA production technique, recent studies have shown the preparation process having a significant role in the MEA final performance ability [6].

2.1.2 Nafion

Sulfonated tetrafluroethylene based fluoropolymer-copolymer, also called Nafion, is the most commonly used membrane in PEMFC [10] (see Figure 2).

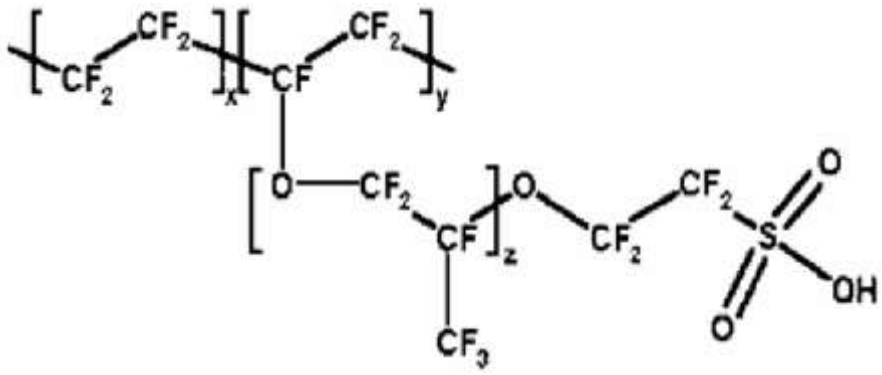

Figure 2: Molecular structure of Nafion

The incorporation of perfluorovinyl ether groups ended with sulfonate groups onto a tetrafluoroethylene (PTFE) backbone gives Nafion its distinct ionic characteristics. Together with exceptional thermal and mechanical stability, Nafion has become a popular PEM material [5, 6].

2.2 Rheology

The study of deformation and flow properties of matter is named rheology [11]. Rheology is the science of deformation of fluids and solids, and can be measured in quantities such as viscosity, elasticity, and yield strength. The flow behaviour of the material is described by viscosity, while the structure of the material is described by elasticity. Materials that show both viscous and elastic properties are called viscoelastic materials, and the rheological properties are regulated by the structure of a material. One can explain and improve both process characteristics and material consistency by knowing the rheological properties and structure of the material [12].

2.2.1 Viscosity

Viscosity, η, is a physical property of liquids and gases that denotes the "thickness" or internal resistance to flow and can be seen as a measure of friction in liquids. Viscosity is defined as the ratio between shear stress, σ, and the rate of shear, dγ/dt. If the material has a fast deformation, high shear rate at small shear stresses, the viscosity is low [13].

$$\sigma = \eta \frac{d\gamma}{dx} \tag{4}$$

The SI-unit for dynamic viscosity is pascal-second (Pa · s), which is equal to 1 N · s / m^2 or 1 kg / (m · s). Some dynamic viscosities for Newtonian liquids can be seen in the table below.

Table 1. Reference data viscosity

Substance	**Viscosity (Pa*s)**
Water	$1{,}002*10^{-3}$
Mercury	$17{,}0*10^{-3}$
Honey	$10*10^{-3}$

2.3 Screen printing

Screen printing is one of several deposition processes used in the production of films. In the sphere of science, thick film hybrids have various potential applications, one of which is in electrochemical systems. To achieve uniformly replicable thick films, the screen-printing method normally consists of five requirements, which are as follows: the proper medium, a mesh screen with a printed stencil pattern, a substrate to print upon, a squeegee, and the ability to secure the base to prevent substrate movement throughout the process.

The printing procedure is represented in three phases in Fig. 3. The initial step is to apply the printing media (ink, emulsion, or paste) to the mesh screen, making sure that it is not in touch with the substrate. Such contact might possibly ruin the print since the substrate would "snap-off" the screen uncontrolled, resulting in a contaminated sample. The printing take place when the squeegee applies pressure across the screen and drives the print medium through the mesh screen, forming the desired pattern in a precise and efficient manner [14]. In this thesis, 55, 63 and 100 mesh silk screens (with 40 × 20 cm^2 area) were used, 25 µm ink and 45 ° angle were used to print the paste on different substrates.

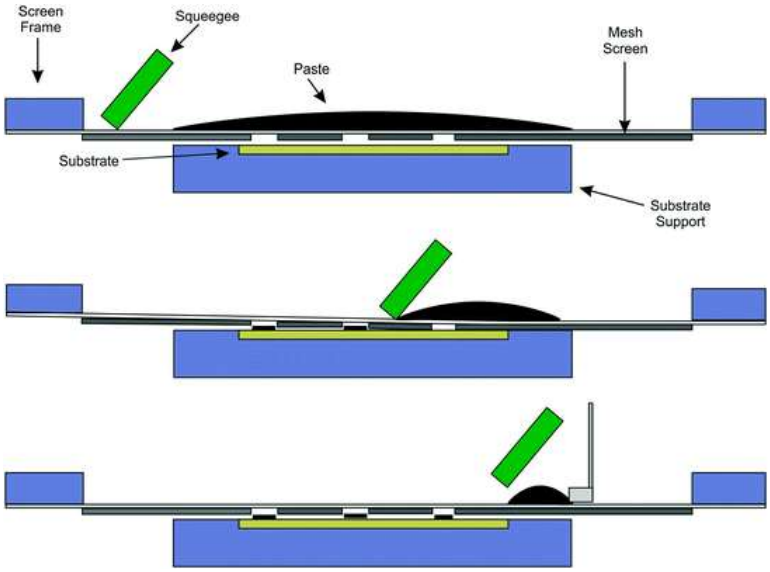

Figure 3: Schematic of the printing process [13a]

3.Instrumental theoretical background

3.1 Light microscopy

Since the naked eye can only detect objects larger than 0.2 mm, numerous microscopical techniques have been developed to improve resolution [15]. A light microscope contains a light source, condensers, and two lenses, one ocular lens and one objective lens, which work together to magnify the sample. A lamp is frequently used as the light source, generating the light required to illuminate the sample. The light is focused onto the sample after passing through the condenser, that concentrates the light from the illumination source. The sample is then enlarged by the lenses and seen using an eyepiece or camera [16]. Bright field is the most used method of light microscopy. By making the item stand out against a bright background it improves tissue observations. This is due to the absorption of a portion of the transmitted light in dense areas.

3.2 Scanning electron microscopy (SEM)

Scanning electron microscopy (SEM) is an imaging method used to visualize surface morphology and topography. By scanning the surface with a focused beam of electrons signals are generated, such as backscattered electrons, secondary electrons and X-rays, which can be detected and transformed into an image. SEM provides high resolution, magnification and focus, as a result, it is appropriate for observing surface structure on a micro- and nanoscale [17].

3.3 Contact angle

The wettability of a surface is measured using contact angle measurements. How a liquid is spread out over a surface is determined by the existing forces between the material and the liquid applied. Hydrogen bonds, van der Waal forces, mechanical and electrostatic forces, to mention a few, all impact wettability. The contact angle is defined as the angle between the solid surface and the liquid droplet surface, see figure 4.

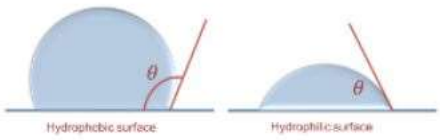

Figure 4: Illustration of a contact angle for a hydrophobic and hydrophilic surface [18]

Depending on the solid's hydrophobicity and the properties of the liquid, different values of the angle are obtained. The value can vary between 0° and 180°. The relation can be described by Young's equation:

$$\gamma^{solid-vapour} = \gamma^{solid-liquid} + \gamma^{liquid-vapour}\cos(\theta) \qquad (5)$$

where θ is the contact angle and γ is the interfacial free energy [19]. A hydrophobic material has a high contact angle, generally larger than 90°, which relates to poor wettability and a low surface free energy. Meanwhile a hydrophilic material has a low contact angle, generally lower than 90°, which means good wettability and a high surface free energy.

3.4 Profilometry

Surface roughness may be measured using a variety of analytical techniques, including optical scanning techniques, scanning probe microscopy, and stylus profilometry. A stylus profilometer detects the 2D surface texture using a stylus tip moving at a constant speed in contact mode [20]. The height of the tip generates an analog signal, which is transformed into a digital signal, analysed, and displayed. A stylus profilometer can detect microscopic vertical features with heights ranging from 10 nanometres to 1 millimetre. The benefits using a stylus profilometer are surface independence, resolution, and the fact that it is a direct method that does not require modelling.

4.Methodology

The method and materials used in this thesis are describe in this section starting with an overview of the whole process, followed by a more detailed description of each step including methods and used instruments and materials. The experimental part can be divided in three phases: broad testing, reproducibility, and characterization, and the overall work process is visualized as a flowchart in Figure 5.

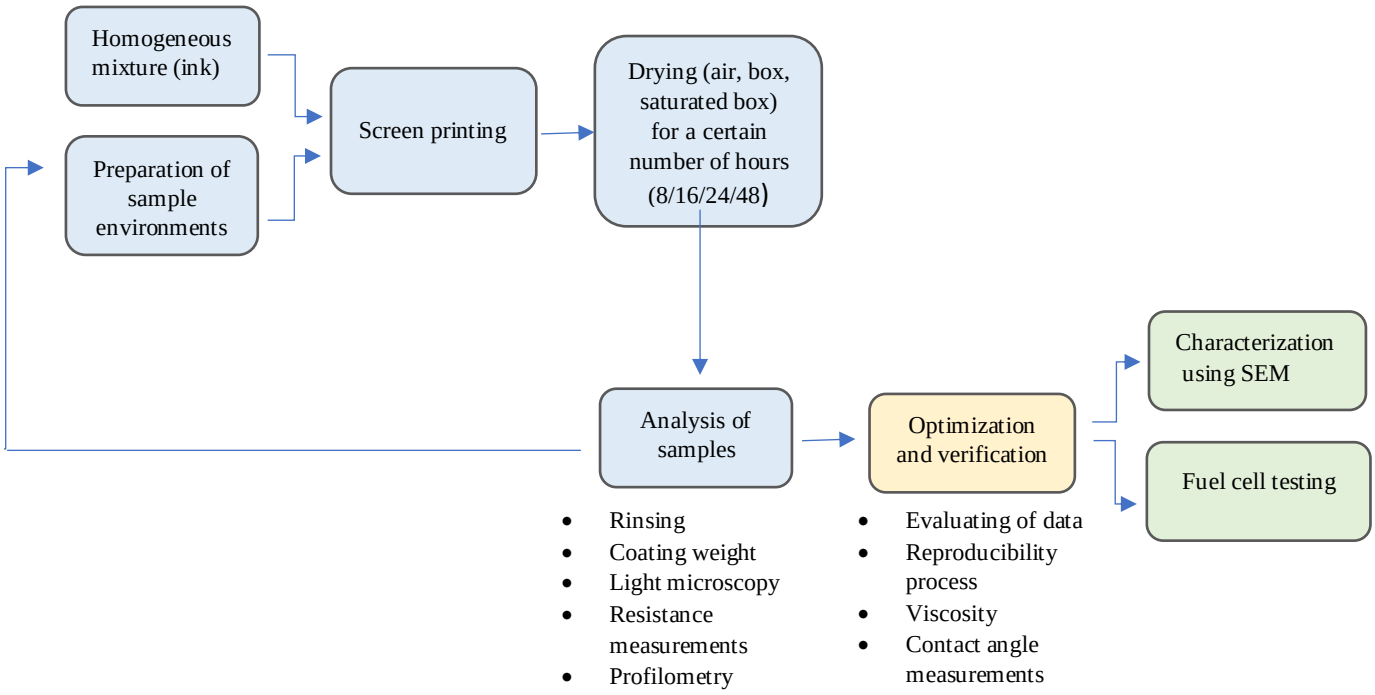

Figure 5. A flowchart illustrating the work process from preparation of screen-printing experiments to the proposal of important drying parameters, their optimal settings, and the performance in the fuel cell.

In phase I (blue), a large number of different tests have been prepared, changing one parameter at the time. The different parameters evaluated in this project are the solvent in the ink, the sample environment, drying time, and the substrate. Each sample has been analysed in the microscope, with the profilometer and by resistance measurement to find which parameters work the best. In phase II (yellow) the parameters have been set and samples in these specific conditions are reproduced to ensure that the result is reliable. Again, each sample is analysed and evaluated in the same way as in phase I. In phase III (green) the samples are further analysed. Fuel cell tests are carried out to see how well the samples perform. Characterization using SEM has also been executed as a complement to previous analysis of the sample.

4.1 Preparation of the ink

Weigh up catalyst powder (batch id used: OMC01H) in a vial and Nafion solution (FuelCell Store D2021, 5% Nafion solution) in a small beaker. In the tiny beaker with Nafion, add drops of dispersant (HyperMer KD2-LQ-/CQ) and mix for 1 minute with the shear mixing machine (EKA UltraThurrax T25ETClean). Then, in three rounds, add the weighted catalyst powder

and stir for 2 minutes at the lowest speed level (3000 rpm) and 1 minute at the next speed level (4000 rpm). Between round 2 and 3, add 1.2 propandiol (PG). In this thesis three separate inks were made, by varying the quantity of PG, resulting in three unique mass percentages: 17.2, 18.3 and 19.6. 17.2, referred to “the original”, is based on an old recipe. 18.3 and 19.6 are modified based on observations and desires to create a more viscous medium, where 19.6 completely lacks PG. If air bubbles were seen in the paste after mixing, sonicate (VWR Ultra Sonic Cleaner) the paste for 5 minutes at level 7 at 23°C.

4.2 Preparation of sample environments

The evaluation of the drying conditions and the drying time was conducted on small lab scale. Samples dried in air without any special treatment were used as reference, and the rest of the samples were dried in a box inside a closable bag (see Figure 6). To create a saturated environment, a filter paper (Munktell, d=70mm) with a solvent (water/PG/1-propanol/ethanol) was added to the box. Also, a few samples were dried inside the box without filter paper to investigate if it was a difference in numbers of cracks in the air-samples depending on fast drying was done.

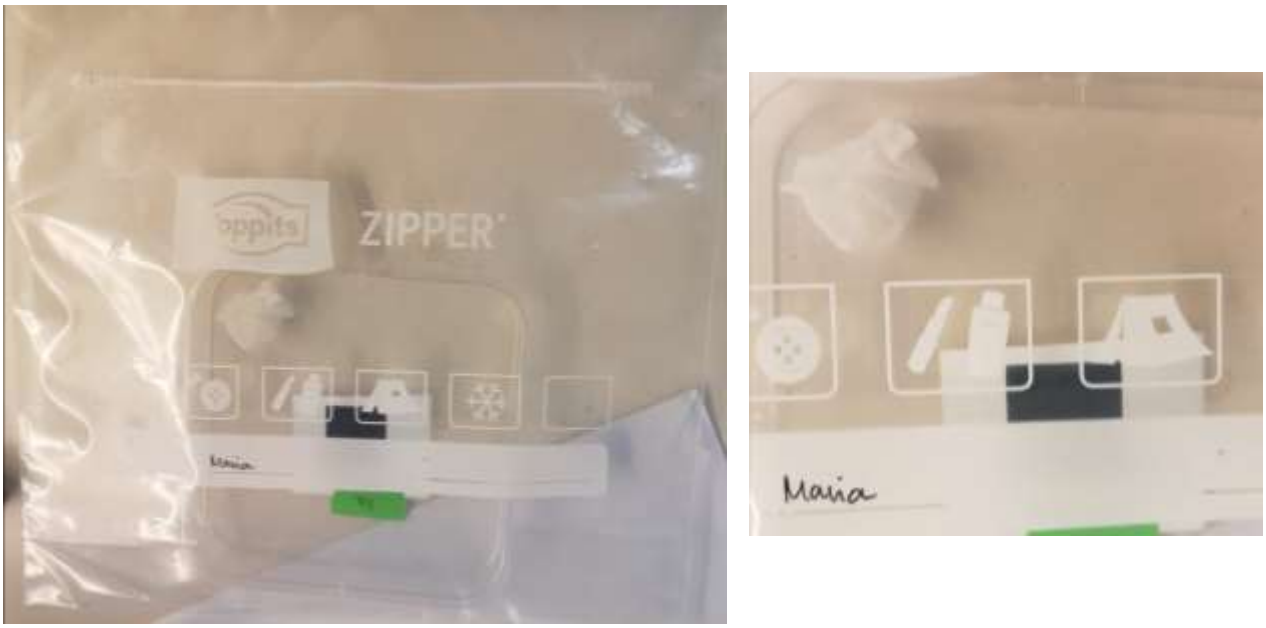

Figure 6: Sample environment with filter paper. Left picture presents the experimental setup and the right one is a zoomed in to visualize the saturated environment and the filter paper closer.

In this experiment, the time parameter was also studied by manufacturing numerous samples in the same environment setup with the difference being in drying times. The drying times investigated in this study were 8/16/24 and 48 h in saturated environment, with a further 24 h hours in slow air-drying environment. In addition to the microscope evaluation each sample was examined to see if it was dry before analysis to determine if a time modification was needed for the following iteration.

4.3 Screen printing

An automatic screen printer (ESC AT-45PAB) was used for all samples with the speed 50mm/sec and maximum squeegee pressure. Three different mesh screens produced by Europa Siebdruck Centrum were used (31-100, 71-055 and 59-063) including two rows of eight squares of 5 cm^2 each. Printing was done on different substrates attached to the screen by tape. The substrates used in this thesis are PET, glossy paper, Toray paper (Fuel Cell Store, MGL190), Teflon-coated Toray paper (Fuel Cell Store, Toray paper 060) and Nafion membrane (Fuel Cell Store, Nafion™ 212). The ink was applied 1 cm from the first square by a spatula. For samples with double layers, a quick clean was made between the prints, to remove paste before drying up and clog the mesh holes. After the print the sample was quickly removed from the screen and placed in the saturated environment in the box. After drying in the box for a certain number of hours, each sample was rinsed in distilled water to remove the PG. During the rinsing procedure each sample was rinsed in a small beaker 10 times, left in another beaker with water for five minutes, rinsed again 10 times in the small beaker and finally left to dry in the fume hood. Once the sample had dried for a few hours the coating weight was measured.

4.4 Light microscopy

Brightfield Transmission Light Microscopy using a Zeiss microscope with an HBO 10 lamp was performed and evaluated with Zen blue edition Zen PRO software. All samples printed on PET or Glossy paper were examined to compare amount and size of cracks and to look closer to the wetting ability of each sample. Samples printed on Toray paper, Teflon-coated Toray paper and Nafion membrane were analysed in SEM instead because the contrast between the substrate and the deposition layer was too small for brightfield light microscopy.

Before collecting microscopic photographs, the whole print was examined, and images were taken at four-five individual locations per sample. These were a) centre b) close to centre c) close to edge d) edge e) corner. Due to the drying atmosphere, all samples showed surface fractures and were rated according to four distinct categories in the matrix below. The samples are graded on a scale 1-5, with 1 being the poorest and 5 being the best. All images in the matrix have a scalebar of 100 micrometres.

Matrix

Cracks

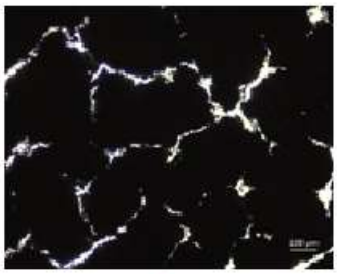

(1)

(2)

(3)

(4)

(5)

Holes/craters

(1)

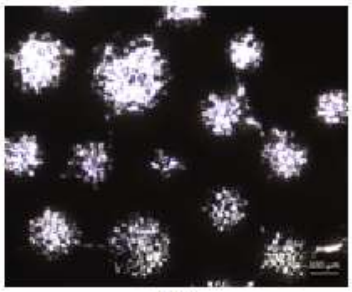

(2)

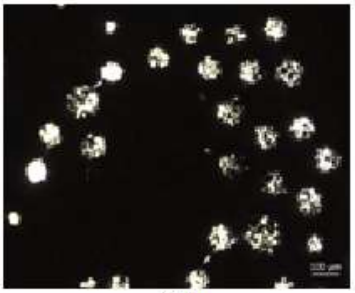

(3)

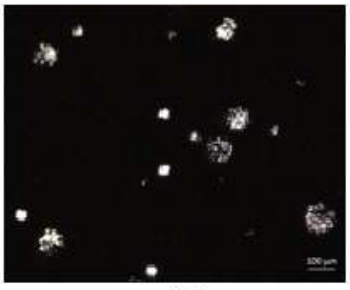

(4)

(5)

Edge quality

(1)

(2)

(3)

(4)

(5)

Ink coverage

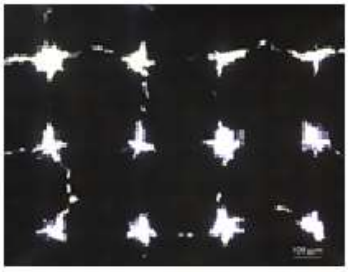

(1)

(2)

(3)

(4)

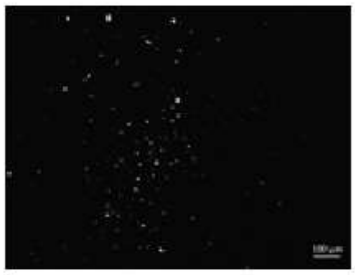

(5)

4.5 Resistivity measurement strategy

Resistivity is the physical property that describes how well a material conducts electricity [21]. A low resistive medium effectively conducts current, whereas a high resistive medium conducts electricity poorly. Resistivity can be determined by measuring the resistance of a sample with a multimeter and taking into account the distance between the contact points and the cross-sectional area of the lead. Every multimeter has two measurement probes and these are placed on the sample and are used to measure how fast electrons travel through the closed circuit at a selected voltage between the two probes. Because the probes of the multimeter have sharp tips, the samples become scratched at contact with the probes. For this reason another type of measurement setup is needed for the printed samples in this thesis.

Aside from not wanting to scratch the coating, it is critical that the distance between the measurement locations is the same for each sample. To match these specifications, a box constructed of plexiglass was built. Plexiglass was chosen because it has a high resistance and thereby affects the measurement of the actual sample material as little as possible. Four holes were made where the tips could be inserted, however the bottom was smooth to prevent surface fractures (see Figure 7). The box was constructed to be the same size as a printed sample, and the distance between each hole was determined to be 8 mm. This was done to ensure that the measurements between the different samples are as equal as feasible. For each sample four measurements were performed (not diagonally) and a mean value was calculated. During the measurements it was important to apply a bit of pressure in order to create a good contact between the box and the sample investigated.

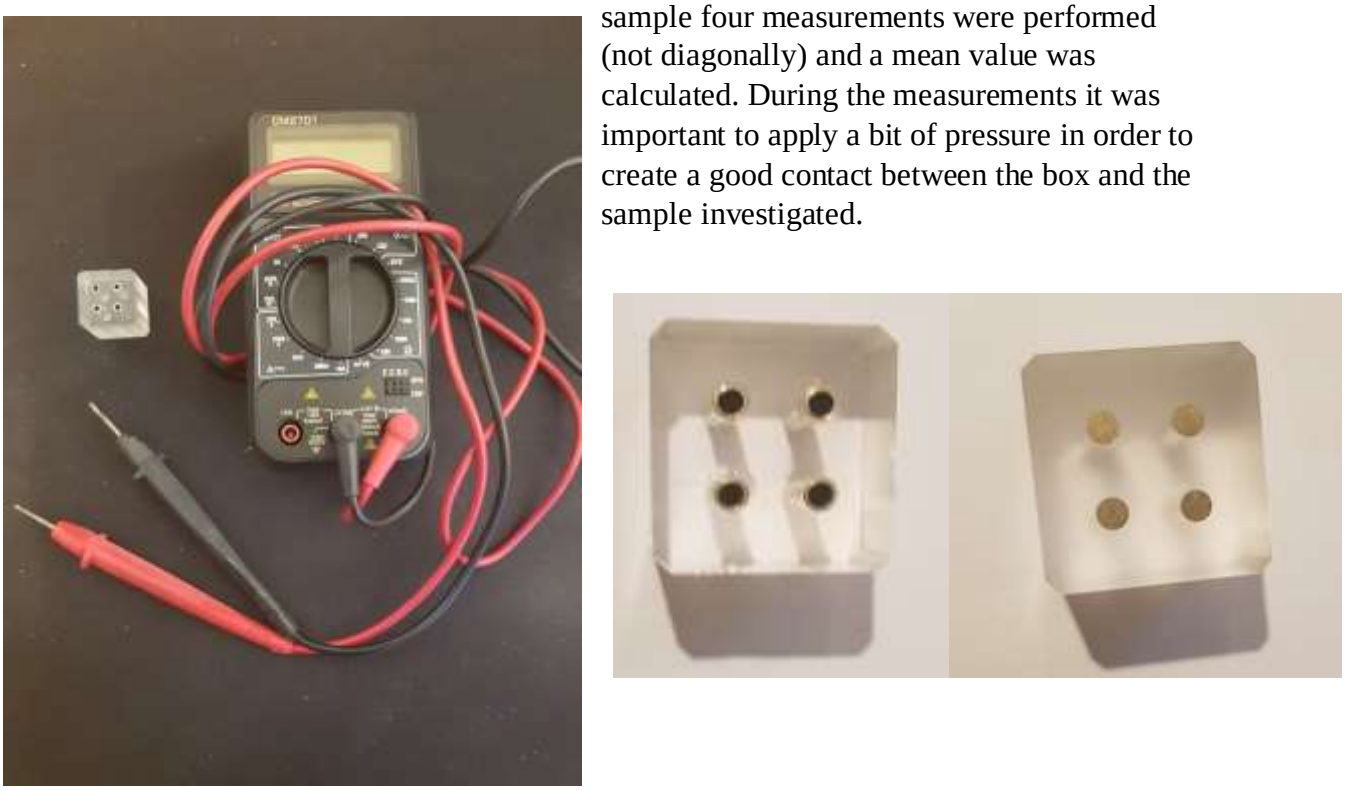

Figure 7: Left picture is an overview of the resistance measurement strategy device. The little box made of plexiglass and the multimeter with adjusted probes to establish a fixed distance of 8 mm. Right picture is a zoom in picture of the plexiglass box, top and bottom.

4.6 Profilometry

The stylus profilometry measurements were performed on a KLA Tencor D-100 profilometer with a pen tip with a radius of 5 µm. The following settings were used: stylus force 0.1, filter layer 8, speed 0.1, and range 100 microns. All samples were measured from the substrate on to the deposition layer and 2-3 mm in. By rotating the sample, each measurement was performed four times to ensure valid results. The four measurements were compared, and the most representative measurement was selected. For additional analysis, the measurement data were plotted once more (see Figure 8), and the mean value and standard deviation were calculated.

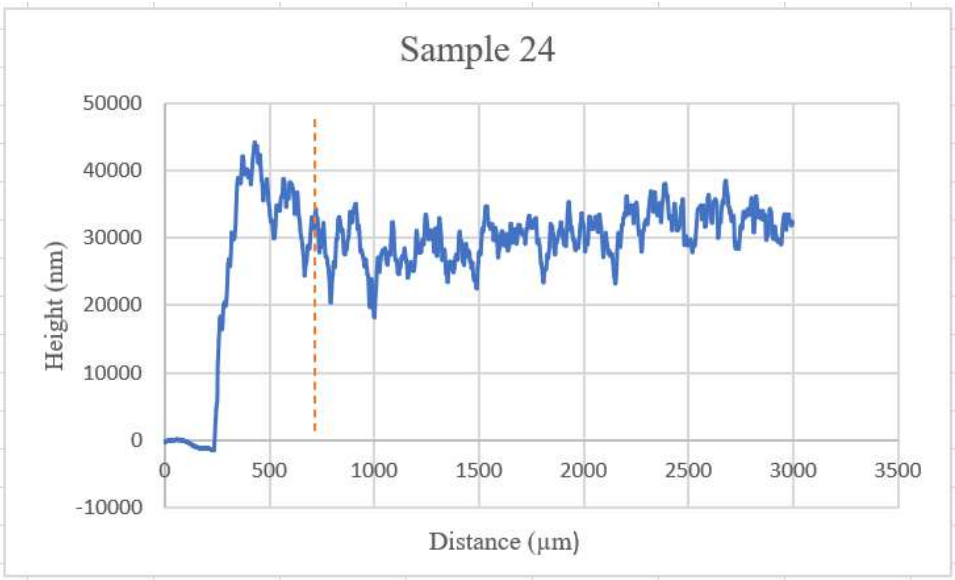

Figure 8: Profilometry measurements on sample 24. The orange line indicates where the sample edge stops and the mean value calculations starts.

5. Results and Discussion

In this section, the results obtained are presented below and discussed throughout. The section is divided into three major parts, broad testing, reproducibility, and characterization. It shall be noted that all samples have been conditioned in room temperature prior to analysis.

5.1 Saturated environment with different solvents

A broad testing in environmental setup was made to understand how the environment influenced the drying procedure, both in time and in numbers of cracks. During the assessment of the samples with microscopic and resistance methods, it was evident the choice of saturated environment was essential in creating a good deposition layer with as few cracks as possible. The results from the different environments can be seen in the graph (Figure 9), where the y-axis shows resistance in kilo-ohm. Low electrical resistance is desirable for high efficiency in energy conversion. The x-axis represents the thickness of the coating layer.

Hao and Cheng as well as several other research groups discuss the importance of creating opportunities for water migration out of the membrane. This is due to the fact that an excessive volume of water increases the likelihood of major fractures and total membrane breakdown [22]. The findings of this thesis are consistent with earlier research. The samples from the aquatic environment revealed significant cracking and, as a result, high resistance values. Samples dried in air or PG showed high resistance values as well and were thus not examined further. Samples dried in an environment with 1-propanol showed initially lower resistance values compared to water, air, and PG. However, the resistance increased at higher mass, which was a less desirable property since in the future, one would like to be able to develop membranes with several layers and varying thicknesses. In this study, samples dried in ethanol produced the greatest results. It was also feasible to see a definite pattern in how larger mass leads to decreased resistance.

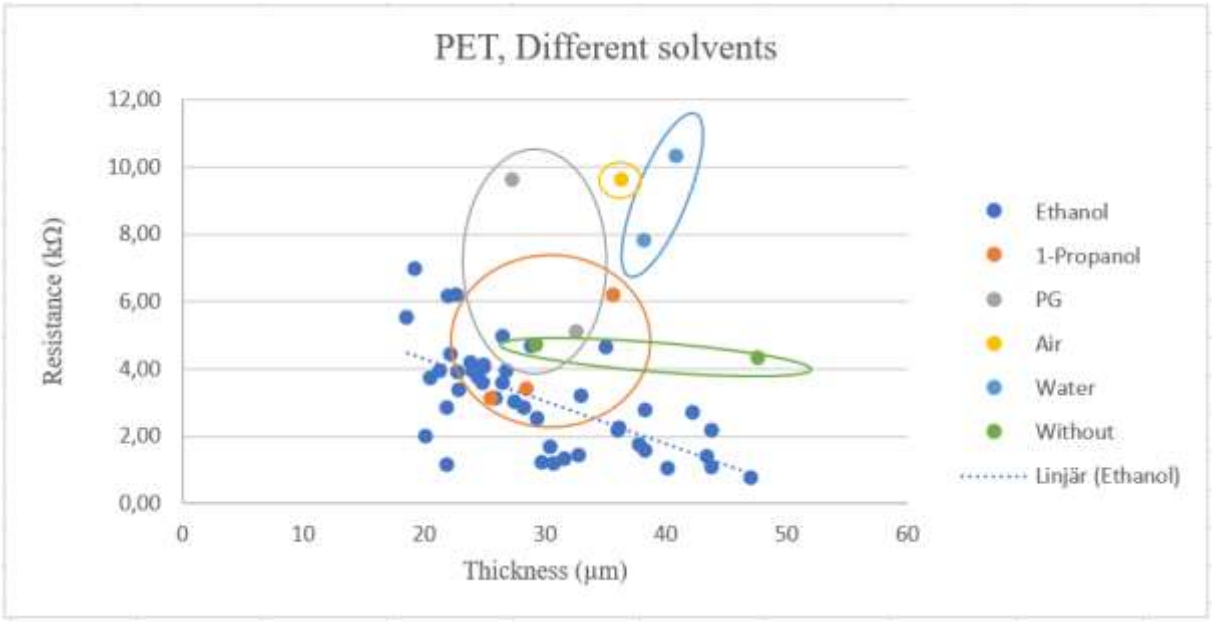

Figure 9: Graph of resistance versus thickness for samples printed on PET and dried in different environments.

5.2 Comparison between different substrates

Part of phase 1, the broad testing, was to investigate how choice of substrate (printer material) influenced the deposition layer in terms of uniform thickness, cracks, and conductivity. In general, resistance measurements reveal that samples printed on PET possess resistance values in the 5-10 kΩ range, in comparison with glossy paper where the range is 6-18 kΩ. By analysing each environment more closely, findings show that all samples of glossy paper have a greater resistance rating than PET. Most obvious in the categories; PG and slow drying in air (without), where the resistance value is twice or higher.

Table 2. Data on thickness and resistance for samples printed on PET. The color code is to cross-reference the samples in the table with figure 9.

Substrate	Solvent	Thickness	Resistance
PET	1-propanol	35,7	6,2
PET	1-propanol	28,5	3,4
PET	1-propanol	25,6	3,1
PET	Air	36,4	9,6
PET	PG	27,3	9,6
PET	PG	32,6	5,1
PET	Without	47,7	4,3
PET	Without	29,3	4,7

Table 3. Data on thickness and resistance for samples printed on Glossy paper. The color code is to compare and cross-reference the samples in the table with samples in table 2.

Substrate	Solvent	Thickness	Resistance
Glossy paper	1-propanol	24,9	5,7
Glossy paper	1-propanol	45,1	7,9
Glossy paper	Air	35,1	10,5
Glossy paper	PG	30,4	17,1
Glossy paper	PG	27,9	9,1
Glossy paper	Without	43,4	8,6
Glossy paper	Without	30,6	15,4
Glossy paper	Without	47,0	8,2

There are several possible reasons why glossy paper performs less well as a printing substrate than PET. The first is the material's hydrophobicity, which causes poorer wetting and the development of air bubbles, which after drying generate craters, holes, and cracks in the coating. The second factor is porosity, which allows ink to penetrate the samples rather than remain on the surface. Meyer, Quentin et al. brings up this issue in their study and also demonstrate how coating on a porous material can result in material losses, resulting in a drop in conductivity [6]. Based on the result presented above, the continuation was constrained to utilizing solely PET as the substrate and printer material for samples made in phase 1 and 2.

5.3 Influence of ink properties

During the reproducibility step, phase II, an overall observation was how different pastes provided different conditions for printing a sample with as much materials as feasible and additionally generate a homogeneous deposition layer. More specifically observations on the original paste (17.2 mass%) was made both during the printing procedure and analysis. Samples made by this paste often exhibit a lower coating weight, less wettability and a higher risk of achieving air bubbles. In contrast to the pastes with 18.3 and 19.6 mass%, both creating a more uniform layer and thicker coating. A viscosity measurement was done on the three distinct pastes to study this further (see Figure 10). The result is consistent with the theory that the higher the mass percent, the higher the viscosity.

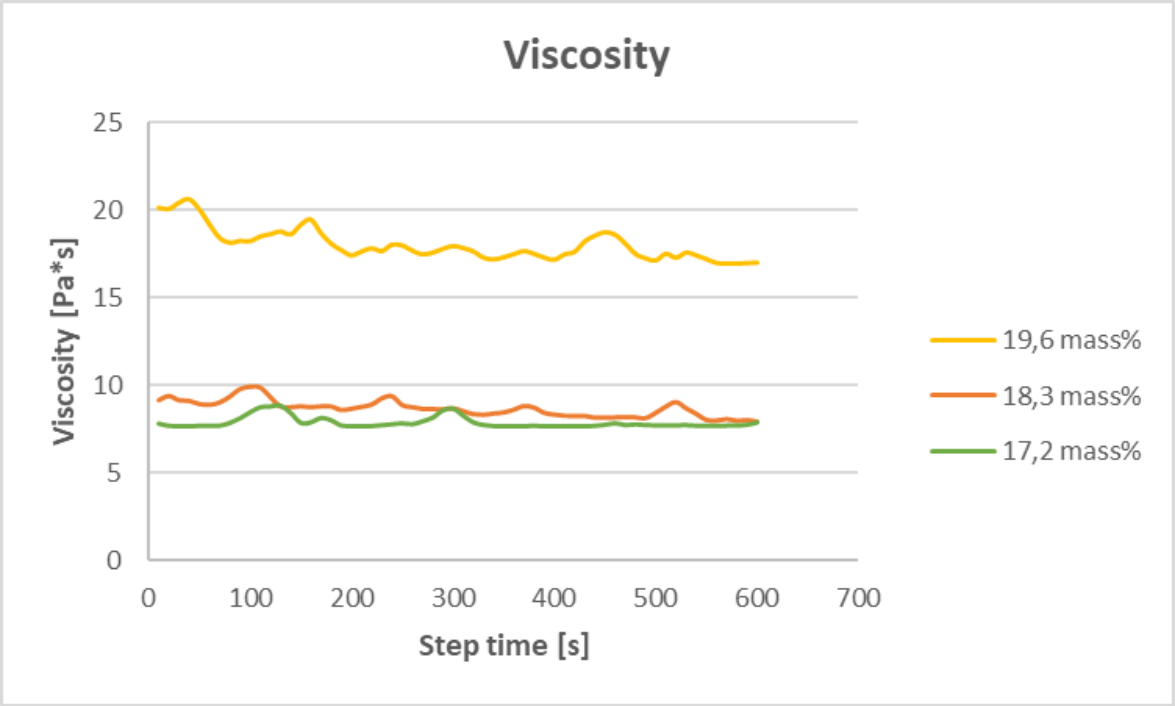

Figure 10: Viscosity measurement of the three pastes. Whereas the original paste is referred to as 17.2 (original), the others are referred to as 18.3 and 19.6. Where the numbers represent the mass percentage of catalyst powder.

The ideal drying conditions, according to this study, were 24 hours in an ethanol atmosphere followed by an additional 24 hours in air environment. The trend seen in Figure 11 indicates that increasing the thickness of the deposition layer generates a decrease in resistance. Figure 11 also demonstrates the variation in thickness and resistance between samples printed with different pastes, where a greater mass percent produces a higher thickness and a lower resistance. The findings may be connected to prior screen-printing research that revealed crucial parameters such as viscosity and loading. To keep the shape of the printed pattern while drying, a paste with a relatively high viscosity is required. Other critical factors are a high solids load and a solvent solution that allows for delayed drying. This is done to minimize fast shrinking of the coating during the drying process, which might result in fractures [23].

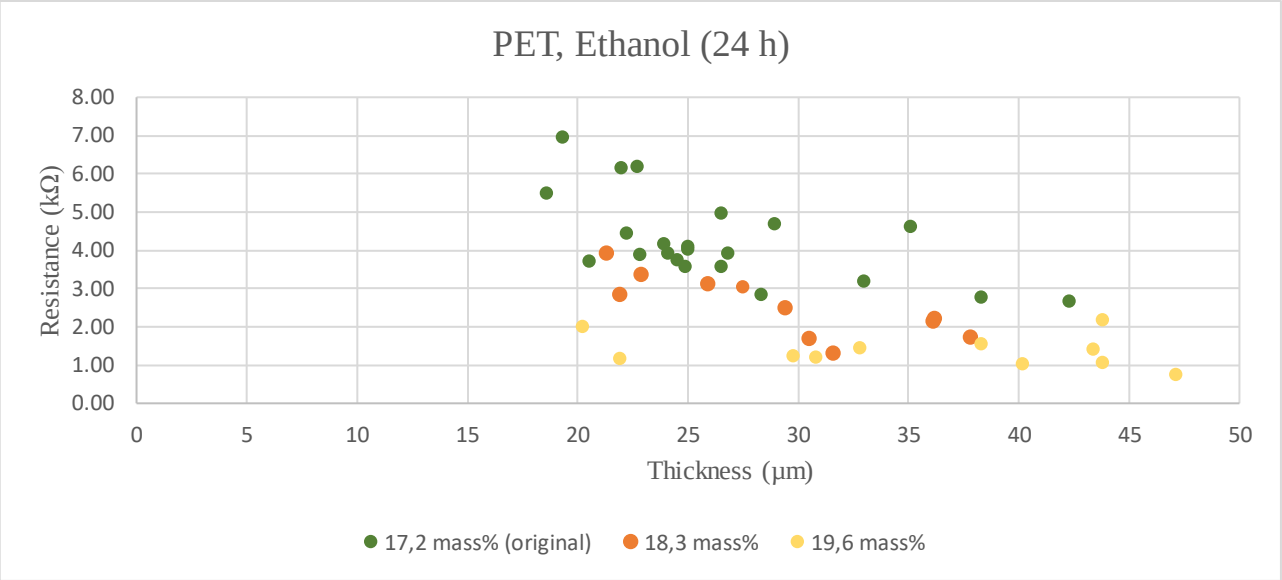

Figure 11: Correlation between thickness and resistance for samples made from three different pastes.

Both Figure 11 and experimental observations point to better results with higher mass%, 18.3 and 19.6 are recommended for further studies. The study also examined how the choice of mesh (55/63/100) affected the thickness of the samples. The data analysis revealed no discernible pattern.

5.4 Fuel cell performance

During the characterisation step, phase III, samples were produced on three separate substrates, each with two layers of coating. For each sample pair, one was dried in air and the other in ethanol followed by slow drying in air. Since earlier results demonstrate the correlation between mass and resistance, an air sample and an ethanol sample were chosen for fuel cell testing based on similarity in coating weight. For each substrate two independent pairs of samples have been run in the fuel cell, a representative sample pair is seen in Figures 12-14. Figure 12 shows fuel cell polarization of three different substrates, illustrating differences in interaction between various printing materials.

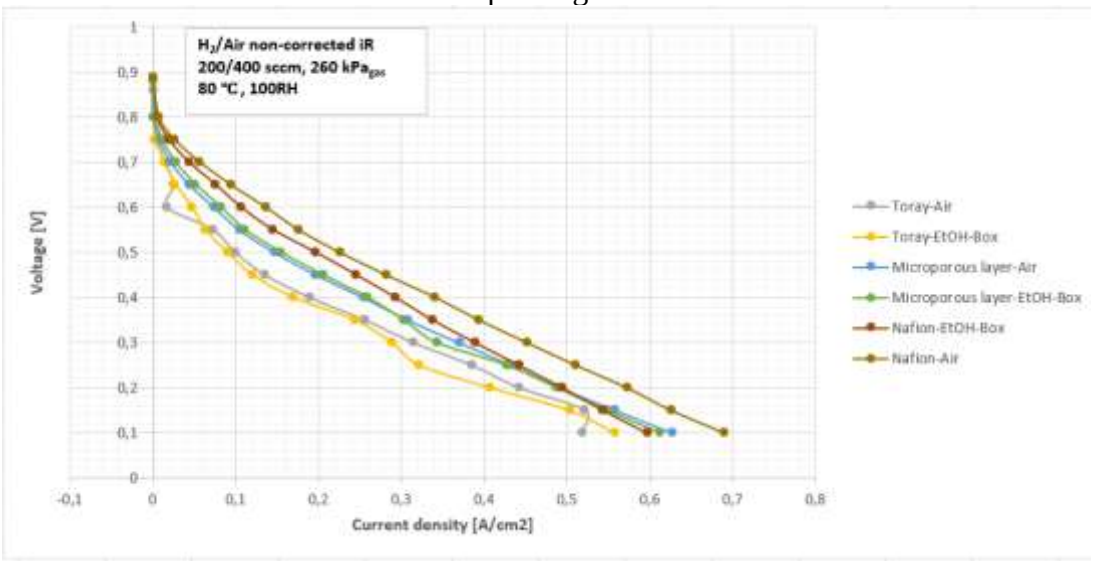

Figure 12: Fuel cell polarization curve of voltage vs. current density showing the impact of activation, Ohmic and transport losses of the six tested samples.

In general all plots in Figure 12 show a typically voltage versus current density trend including activation, followed by the ohmic loss region and then the mass transport loss region. All samples exhibit a negative trend in voltage in the ohmic loss region. The results demonstrate no significant differences between samples dried in air compared to samples dried in ethanol when printed on GDL materials. For the samples printed on Nafion the air-dried samples perform slightly better than the sample dried in presence of ethanol vapour. However, further trials should be conducted before reaching any firm conclusions.

Figure 13 illustrates how the power density of the various materials compare to each another. Samples printed on Toray have the lowest power density values, whereas samples printed on Nafion have the highest. However, it should be highlighted that the samples printed on the Nafion membrane were extremely fragile, and several of the duplicates collapsed during drying or pre-treatment prior to the fuel cell experiments. The samples printed on the microporous layer of the GDL have values somewhere between and also produced findings that were remarkably similar when dried in air and ethanol. The findings were also comparable between the two test cycles. However, the Toray and Nafion samples were not as consistent. Several curves exhibited an uneven behaviour, which may be attributed to poor contact between the layers of the membrane electrode assembly.

Figure 13: Fuel cell power density vs. current density of the six tested samples.

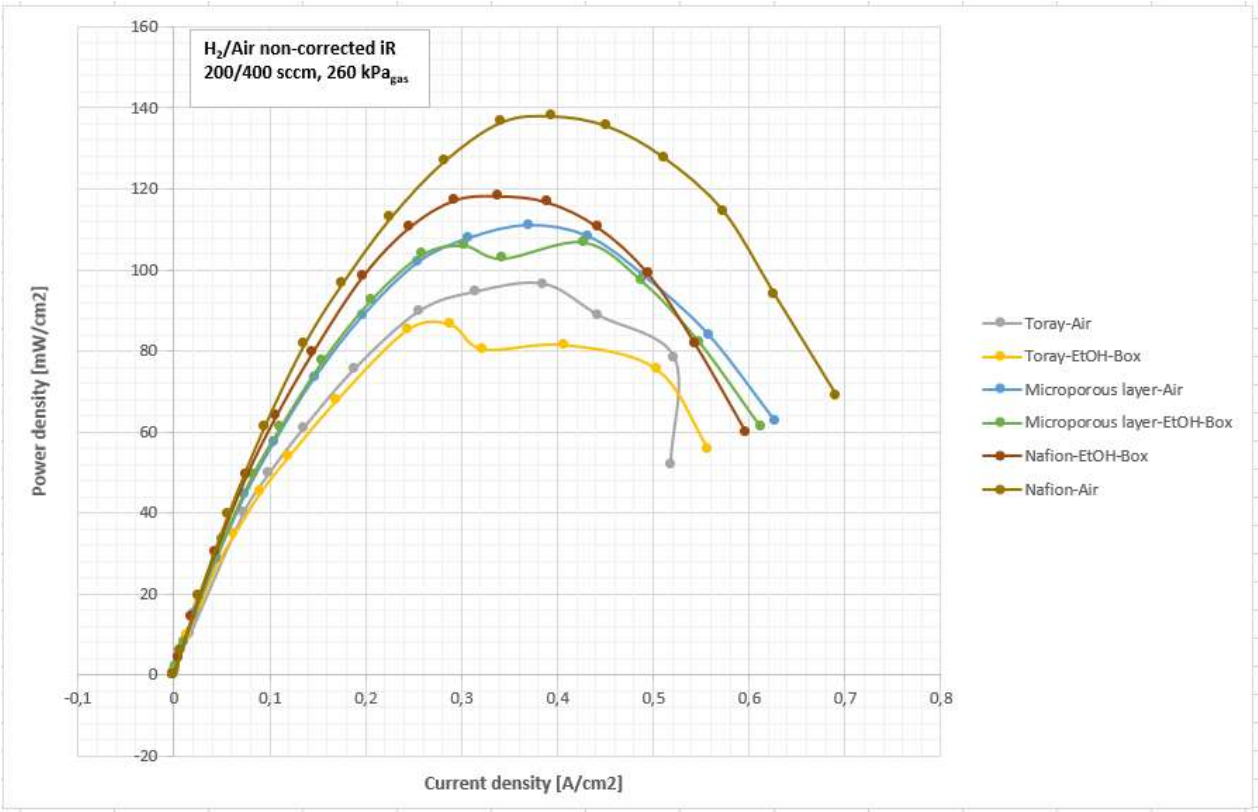

High frequency resistance (HFR) is a measurement obtained at high frequencies (usually above 1 kHz) that represents the ion transport resistance in the membrane electrode assembly. HFR is therefore also an indicator of the membrane water content. It is typically used for fuel cell state-of-health monitoring and a crucial indication of dehydration (low water content of the polymer electrolyte) or flood (too much inside fuel cell electrodes). Excessively high or low HFR values in either direction might indicate various forms of fuel cell breakdown [18].

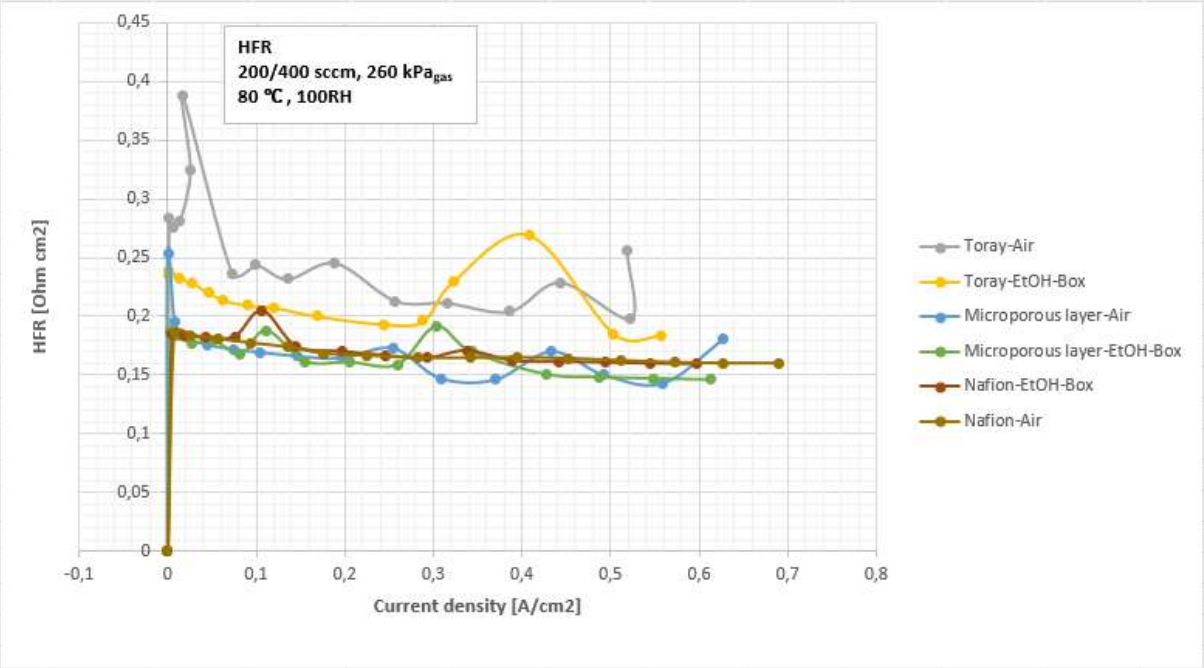

Figure 14: HFR vs. current density of the six tested samples.

5.5 Analysis of the surface and cross-sectional area with scanning electron microscopy

SEM analysis revealed two trends for all substrates (see Figure 15a-c, where 15b and 15c can be found in Appendix A1). First, all air samples suffered from increased fracturing, both in quantity and size. Samples dried in boxes had fewer fractures but more craters and holes. Several of the holes displayed a regularity, and calculations indicated that the holes match the pattern of the mesh, *i.e.* they are 106 micrometres apart.

The deposition layer had a crystal-like surface, while the GDL substrates Toray and Microporous layer on GDL had a clear fibre structure on the images. The Nafion membrane was more compact, and no distinctive microstructure could be discerned.

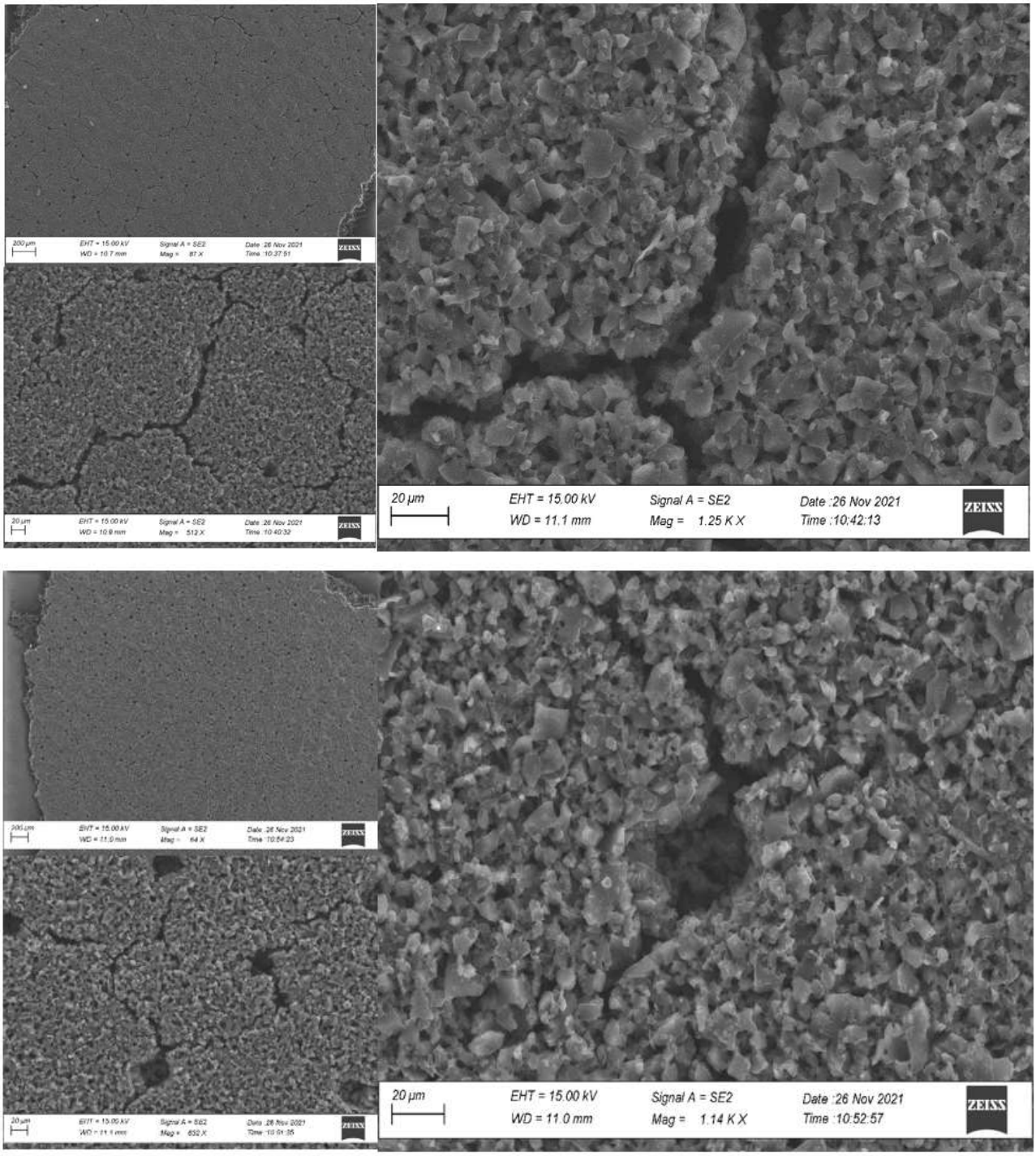

Figure 15a: SEM images in the plane; top three pictures are images on samples printed on Toray paper dried in air; bottom three are images on Toray paper dried in an ethanol atmosphere.

Particles representing the coating and carbon fibres of the GDL substrate are clearly visible in the cross-sectional photographs of the Toray samples. However, the coating in the air sample is more defined than in the ethanol sample, which has a more uneven layer with carbon fibres and particles alternating (see Figure 16). As with the glossy paper samples, we can visibly see how the ink penetrates the Toray sample dried in ethanol, indicating a thinner coating and an inhomogeneous layer (follow the green line in the lower image to the right). The amount of drying time might be one explanation for observing this in the ethanol sample but not in the air. The air sample dries in 4 hours vs 48 hours for the ethanol sample, giving it more time to infiltrate the substrate. Material losses might explain why fuel cell capacity is deteriorating [6]. The less homogenous layer might also be to blame for the flattening of the fuel cell graphs in some of the samples' behaviour.

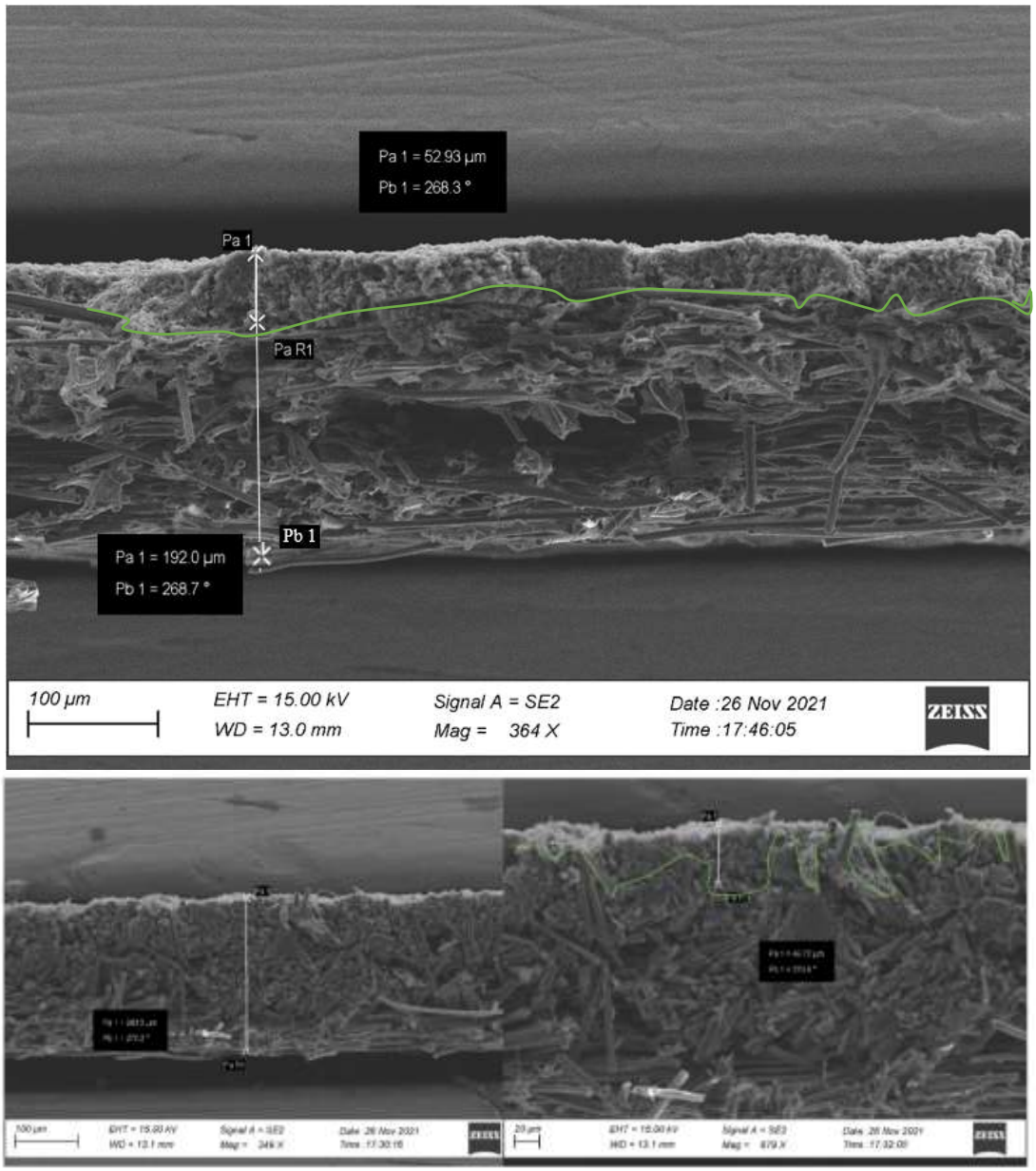

Figure 16: Images of the cross-sectional area for samples printed on Toray; top picture is in air and the two at the bottom is in ethanol atmosphere. The green line shows how the coating is distributed in the sample.

On the other hand, the research group of Kaufman et al have looked more closely at the performance of crack formation in relation to water migration. A completely compact sample where the water has nowhere to go can cause serious flooding, leading to breakthrough failure [24]. Odne et al. presents similar results where a controlled number of channels or cracks proved to be good as liquid water breakthrough points decreased [25].

Shangguan et al. reveal in their work how the incorporation of a sublayer can inhibit ink penetration into the substrate. The loss of active catalyst is therefore minimized. This project's second substrate, a microporous sublayer of the GDL, is exactly the type of sublayer that Shangguan is referring to [26]. The SEM scans show two fine layers that do not permeate each other (see Figure 17). However, the coating is slightly thinner, maybe owing to the hydrophobic surface, which makes it more difficult for the ink to remain on the surface during the printing process. Both SEM analysis and profilometer measurements on this substrate produce highly comparable findings for both samples, which may explain why the fuel cell results are consistent (Figure 12).

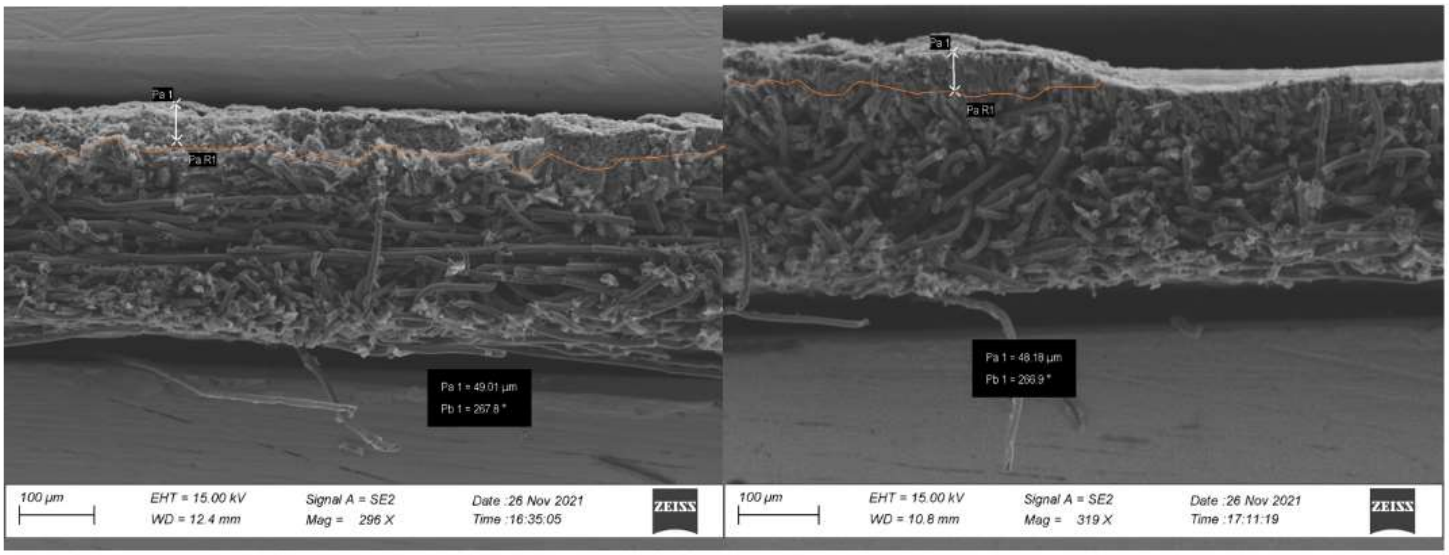

Figure 17: Images of the cross-sectional area for samples printed on Microporous sublayer on GDL; left picture is in air and right is in ethanol atmosphere. The orange line shows how the coating is distributed in the sample.

The third substrate, the Nafion membrane, was extremely fragile, and numerous samples cracked during printing or pre-treatment, as explained previously. Even the best samples were not fully smooth before the fuel cell tests, and a common tendency while drying was that it curled up and created an uneven surface. Cross-sectional photos of the Nafion samples dried in air revealed craters and holes on the surface (green arrows, top right picture in Figure 18) and cracks from the interior (yellow arrows, top left picture in Figure 18), which may suggest poor adhesion. The Nafion sample dried in ethanol atmosphere demonstrated a waffle-patterned surface with a spacing between the peaks measured to about 106 microns, indicating that it was caused by the screen during printing. On the surface, we detect craters and holes, as well as indicators of poor adhesion, as we did with the air sample. Three yellow arrows are shown in the lower right photograph, indicating signs of poor adherence. In comparison to the air sample, this deposition adopts diverse shapes and grows to a larger size several times. The reduced contact may be the reason why the ethanol sample performed worse in the fuel cell.

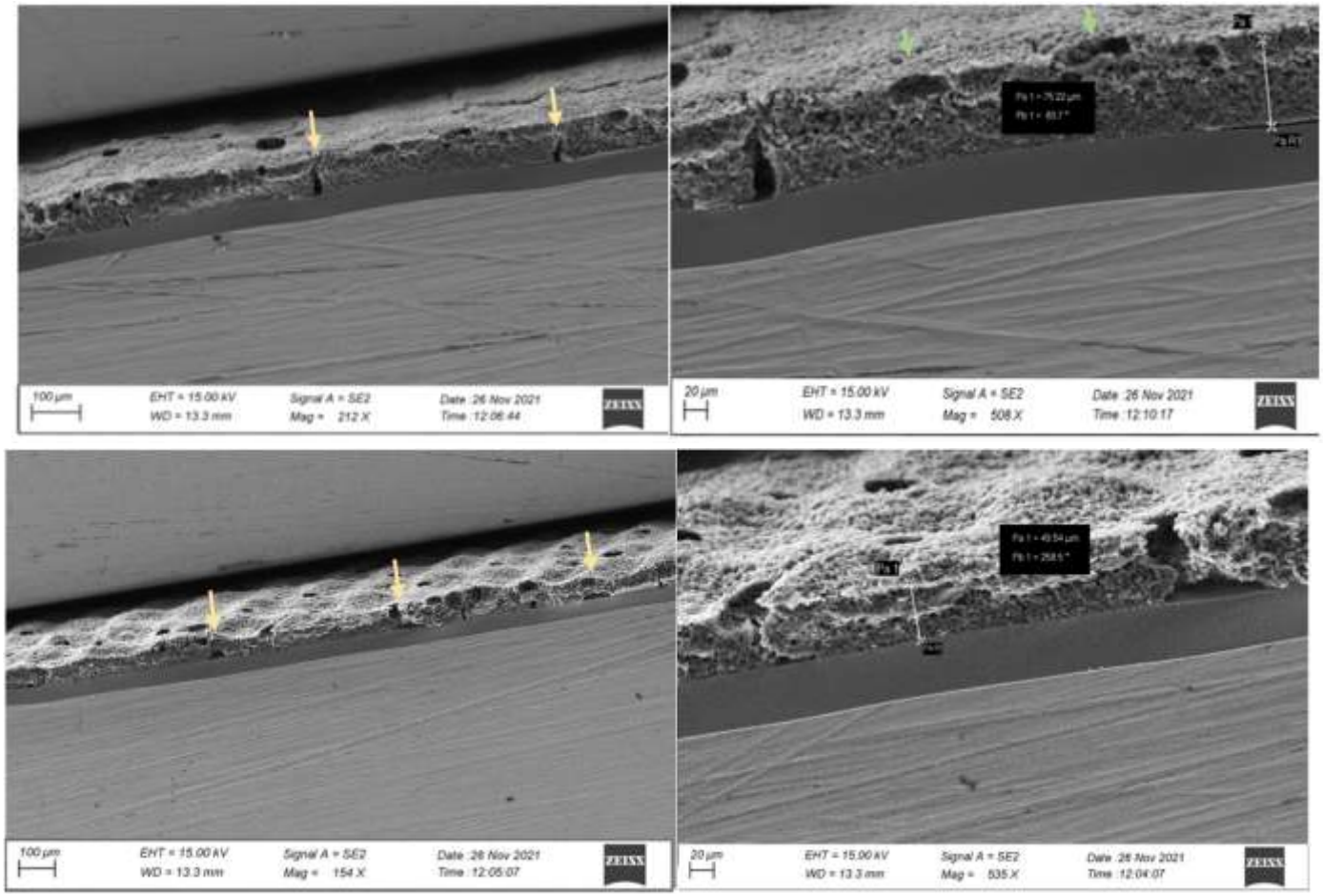

Figure 18: Images of the cross-sectional area for samples printed on Microporous sublayer on GDL; left picture is in air and right is in ethanol atmosphere. The orange line shows how the coating is distributed in the sample.

6. Conclusions

The broad testing experiment indicated that the drying environment and time had an influence on the formation of cracks in the plane. Water, air, and PG fared the poorest, with ethanol proving to be the best of the evaluated options. The optimal settings in this study were 24 hours drying in ethanol followed by 24 hours of slow drying in air. A decreased ohmic resistance can be obtained by increasing the thickness of the deposition layer. The properties of the ink were also discovered to have a significant impact on resistance. Enhanced mass percent contributed to an increased viscosity which aided the screen-printing operation by allowing more ink to remain on the sample, resulting in a thicker deposit layer and fewer cracks.

This thesis also looked at the substrate selection in greater depth. When utilizing a porous substance, such as Glossy paper or Toray paper, a portion of the ink may penetrate the substrate rather than staying on the surface as a coating. In these circumstances, the drying process benefits from a faster drying period to reduce the loss of active catalyst. On the other hand, previous research has shown that controlled cracking or the creation of channels can be positive for the transport of excess water and reduce the risk of total collapse of the membrane. If one study the resistance perpendicular to the plane, both cracking and porosity can be beneficial. Another option is to employ a microporous sublayer as a membrane that inhibits ink from entering the substrate. A desirable mechanical property of the MEA is also attained by adding an additional polytetrafluoroethylene sheet. However, the more hydrophobic surface creates additional printing issues since the ink is more difficult to keep in the desired sample pattern.

The Nafion membrane was the third substrate tested, and it proved to be extremely fragile. Several samples cracked before being tested in the fuel cell. The samples that made it all the way through, on the other hand, performed well in relation to other substrates. Holes, craters, and cracks may be detected in Nafion samples using SEM analysis, in similarity to the finding in the other substrates. However, the Nafion samples suffered interior defects as well. The interior cracks imply less good adhesion and, in the long term, poorer contact in the fuel cell, which may explain the Nafion tests' inconsistent findings. Fuel cell tests show a better performance for Nafion dried in air but since several samples cracked a controlled drying procedure could be positive.

7. Future prospects

The findings from this research reveal that numerous elements, such as ink, drying environment, and substrate selection, may have a significant impact on the membrane electrode assembly. In future research, it would be interesting to further optimize the qualities and identify the correct ink in connection to the right environment and substrate choice.

In terms of substrates, the Nafion membrane was the most unpredictable material, but it was also the substrate with the most potential. Another possible extension would be to look at the best approach to pre-treat the Nafion membrane to avoid the probability of it being damaged during drying or pre-treatment to the fuel cell testing. An additional path for the development of the Nafion membrane is to have a better knowledge of the adhesion strength and what influences it.

SEM analysis revealed screen-printing marks, notably mesh holes, on all surfaces examined. The data and findings acquired in this experiment cannot indicate if these formations have a good, negative, or insignificant effect on performance. A possible continuation is to gain a better knowledge of how this impacts the performance of the substrates and how to regulate these prints.

References

[1] https://blogg.wwf.se/2019/03/05/befolkningsokningen-ar-vi-for-manga/

[2] R.Jasinski, Nature, 1964, 201, 1212.

[3] J.K.Dombrovskis, Doktorsavhandlingar vi Chalmers tekniska högskola, 2016

[4] Van der Linden, Pahon, Morando and Bouguain, Vehicle Power and Propulsion Conference, 2020

[5] Pierre Toudret, Jean-Francois Blanchot, Marie Heitzmann and Pierre-Andre Jacques, Impact of the Cathod Layer Printing Process on the Performance of MEA Integrating PGM Free Catalyst, Catalysts 2021, 11, 669, DOI: https://doi.org/10.3390/catal11060669.

[6] Meyer, Quentin et al. "Investigation of Hot Pressed Membrane Electrode Assemblies using X-ray Computed Tomography." (2018).

[7] Zhongwei.Chen, Jean-Pol Dodelet and Jiujun Zhang, Non-Noble Metal Fuel Cell Catalysts, 2011

[8] Powercell webside, Technology, How does fuel cell work?, https://powercell.se/en/how-do-fuel-cells-work

[9] Cheng Yang, Ning Han, Yajun Wang, Xiao-Zi Yuan, Jiaoyan Xu, Henghui Huang, Jiantao Fan, Hui Li, and Haijiang Wang, A Novel Approach to Fabricate Membrane Electrode Assembly by Directly Coating the Nafion Ionomer on Catalyst Layers for Proton-Exchange Membrane Fuel Cells, ACS Sustainable Chemistry & Engineering 2020 8 (26), 9803-9812 DOI: 10.1021/acssuschemeng.0c02386

[10] Bernard Bladergroen, Huaneng Su, Sivakumar Pasupathi and Vladimir Linkov, Overview of Membrane Electrode Assembly Preparation Methods for Solid Polymer Electrolyte Electrolyzer, SAIAMC, University of the Western Cape, South Africa, DOI: http://dx.doi.org/10.5772/52947.

[11] Duncan J. Shaw, Introduction to Colloid and Surface Chemistry, Third Edition, Oxford, 1980, ISBN: 0 7506 0338 0

[12] Marcelo Tramontin Souza, Igor Maia Ferreira, Elisângela Guzi de Moraes, Luciano Senff, Antonio Pedro Novaes de Oliveira, 3D printed concrete for large-scale buildings: An overview of rheology, printing parameters, chemical admixtures, reinforcements, and economic and environmental prospects, Journal of Building Engineering, Volume 32, 2020, 101833, ISSN 2352-7102, DOI: https://doi.org/10.1016/j.jobe.2020.101833.

[13] Haiyang Yang et al. "A novel method for determining the viscosity of polymer solution". In: *Polymer Testing* 23.8 (2004), pp. 897–901. issn: 0142-9418. doi: https://doi.org/10.1016/j.polymertesting.2004.05.005.

[14] Foster C.W., Kadara R.O., Banks C.E. (2016) Fundamentals of Screen-Printing Electrochemical Architectures. In: Screen-Printing Electrochemical Architectures. SpringerBriefs in Applied Sciences and Technology. Springer, Cham. DOI: https://doi.org/10.1007/978-3-319-25193-6_2.

[15] Yang, R. 2018. Microscopic Analysis. Analytical Methods for Polymer Characterization. 1 ed. Boca Raton: CRC Press.

[16] D. B. Murphy and M. W. Davidson, Fundamentals of Light Microscopy and Electronic Imaging: Second Edition, John Wiley and Sons, 9 2012, DOI:10.1002/9781118382905.

[17] R. Yang, Analytical methods for polymer characterization, 2018

[18] T.Lin, L.Hu, W. Wisely, X.Gu, J. Cai, S. Lister and L.B.Kara, "Prediction of high frequency resistance in polymer electrolyte membrane fuel cells using long short term memory based model", Energy and AI 3 (2021), 100045, DOI: https:/doi.org/10.1016/j.egyai.2020.100045.

[19] Raziyeh Akbari, Carlo Antonini. "Contact angle measurements: From existing methods to an open-source tool". In Advances in Colloid and Interface Science 294 (2021), 102470, issn: 0001-8686, https://doi.org/10.1016/j.cis.2021.102470.

[20] Lee, D.-H.; Cho, N.-G.. Measurement Science and Technology, October 2012, 23(10), Institute of Physics Publishing DOI: 10.1088/0957-0233/23/10/105601.

[21] Nationalencykopedin, resistans, https://www.ne.se/uppslagsverk/encyklopedi/l%C3%A5ng/resistans

[22] Zhou, C.; Guo, L.; Chen, L.;Tian, X.; He, T.; Yang, Q. Pore-Scale Modeling of Air–Water Two Phase Flow and Oxygen Transport in Gas Diffusion Layer of Proton Exchange Membrane Fuel Cell. Energies 2021, 14, 3812. DOI: https://doi.org/10.3390/en14133812.

[23] Lisa Palmqvist, Report Powder Processing Assessment for MIL project, Department of Applied Chemistry, Chalmers, November 2016

[24] Zhigang Qi, Arthur Kaufman, Improvement of water management by a microporous sublayer for PEM fuel cells, Journal of Power Sources, Volume 109, Issue 1, 2002, Pages 38-46, ISSN 0378-7753, https://doi.org/10.1016/S0378-7753(02)00058-7.

[25] Odne S. Burheim, Gregory A. Crymble, Robert Bock, Nabeel Hussain, Sivakumar Pasupathi, Anton du Plessis, Stephan le Roux, Frode Seland, Huaneng Su, Bruno G. Pollet, Thermal conductivity in the three layered regions of micro porous layer coated porous transport layers for the PEM fuel cell, International Journal of Hydrogen Energy, Volume 40, Issue 46, 2015, Pages 16775-16785, ISSN 0360-3199, https://doi.org/10.1016/j.ijhydene.2015.07.169.

[26] Z.Shangguan, B.Li, P.Ming and C.Zhang, Understanding the functions and modifications of interfaces in membrane electrode assemblies of proton exchange membrane fuel cells, Journal of Materials Chemistry A, 2021, 9, 15111, DOI: 10.1039/d1ta01591e

Appendix

A1: SEM pictures in plane

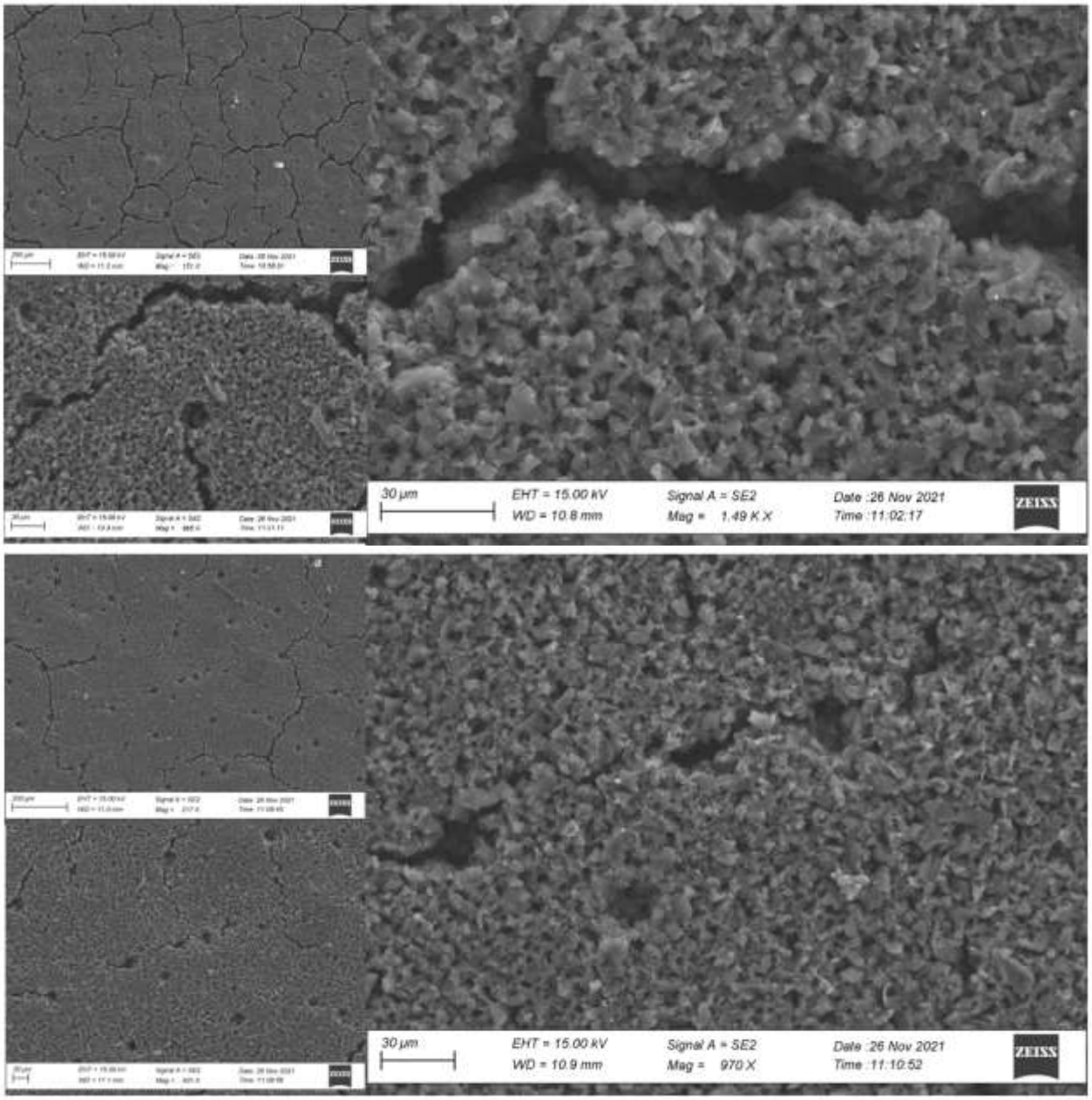

Figure 15b: SEM images in the plane; top three picture are images on samples printed on Microporous layer on GDL dried in air; bottom three are images on samples printed on Microporous layer on GDL dried in an ethanol atmosphere.

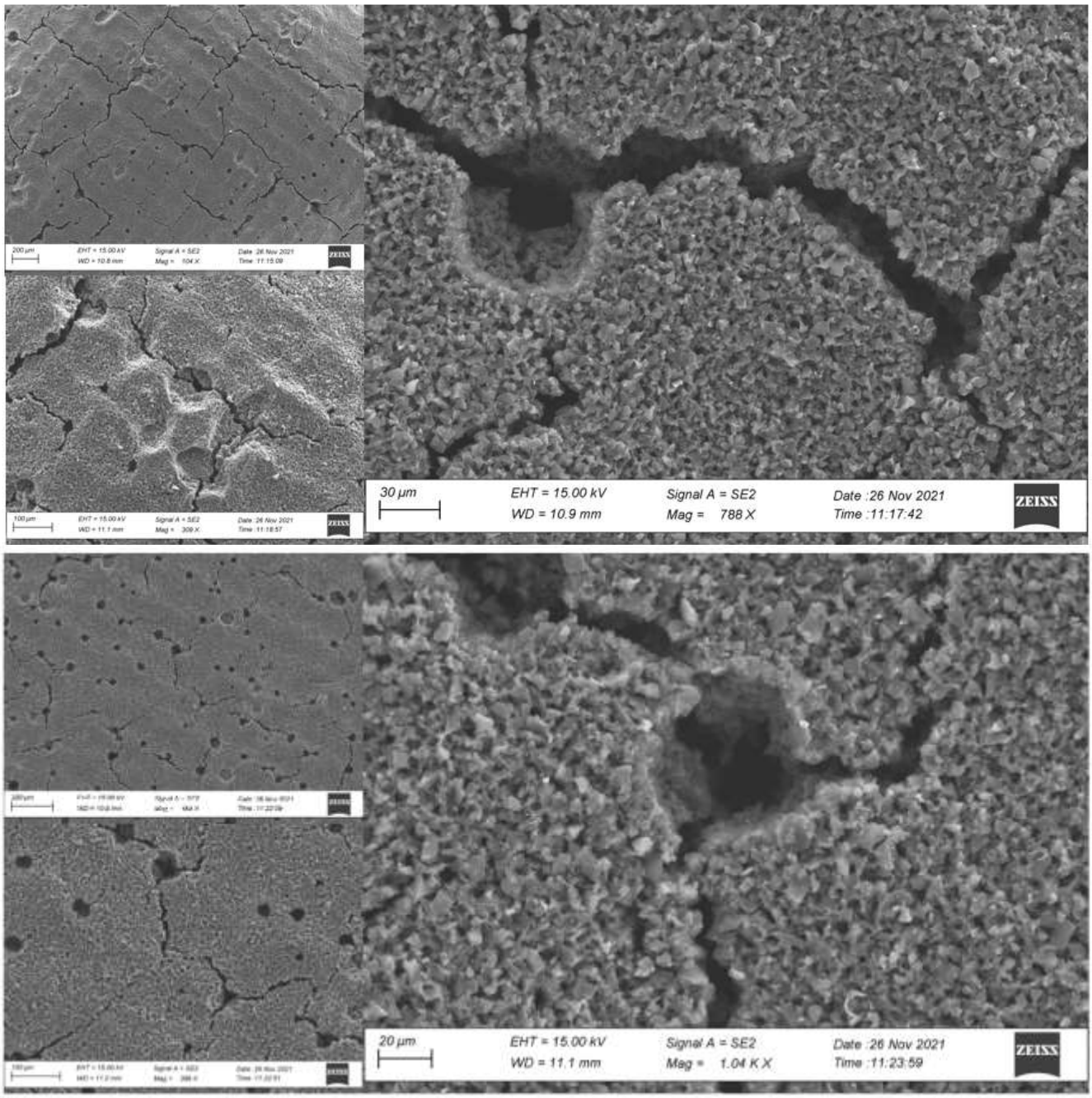

Figure 15c: SEM images in the plane; top three picture are images on samples printed on Nafion membrane dried in air; bottom three are images on samples printed on Nafion membrane dried in an ethanol atmosphere.

A2: Contact measurement angle

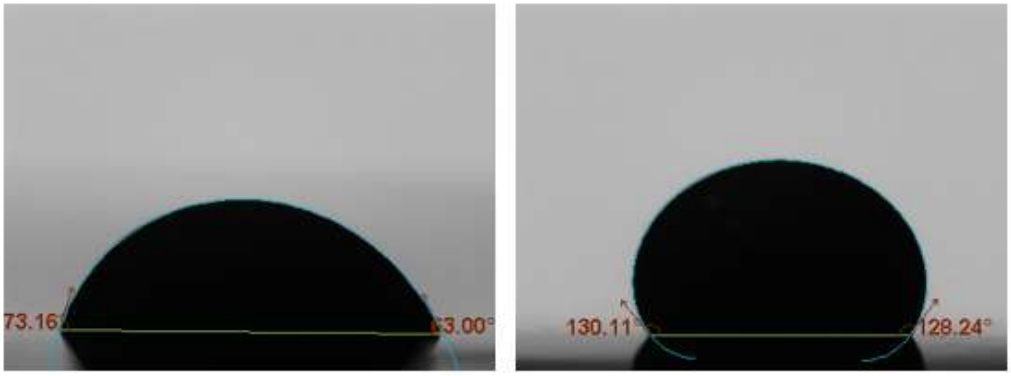

Figure 19: Contact angle measurements. To the left PET and to the right Glossy paper.

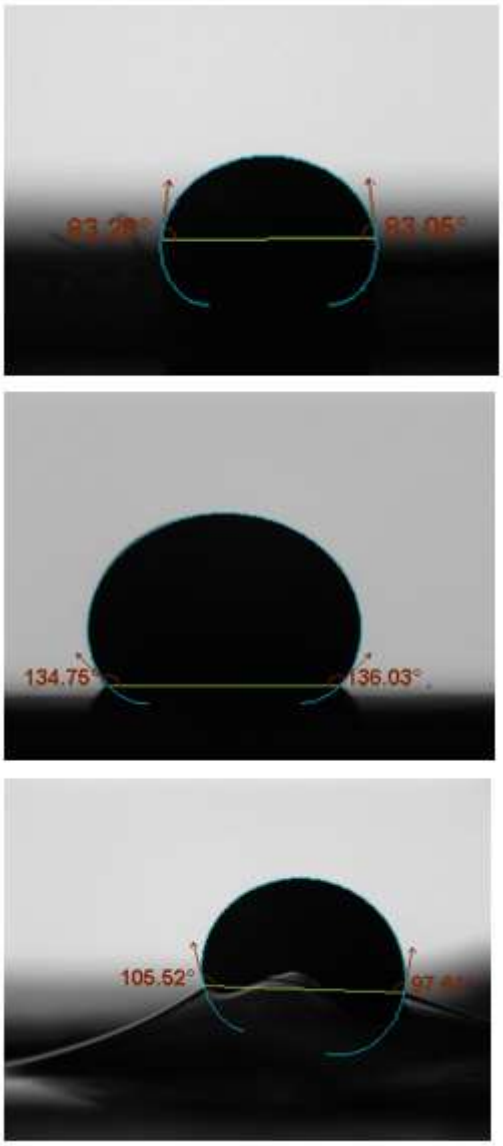

Figure 20: Contact angle measurements. From the top and down; Toray, Microporous layer and Nafion membrane.

Table 4. Density for the coating layer printed on different substrates

Name	**ρ (g/cm^3)**
Toray, air	0,94
Toray, EtOH	1,12
Microporous layer, air	0.667
Microporous layer, EtOH	0,747
Nafion, air	0,440
Nafion, EtOH	0.862